Atmospheric Environment 218 (2019) 116950

Contents lists available at ScienceDirect

Atmospheric Environment

journal homepage: www.elsevier.com/locate/atmosenv

Influences of planetary boundary layer mixing parameterization on summertime surface ozone concentration and dry deposition over North China

Yuanhong Zhao[a,1], Lin Zhang[a,*], Mi Zhou[a], Dan Chen[b], Xiao Lu[a], Wei Tao[c], Junfeng Liu[d], Heng Tian[a], Yaping Ma[a], Tzung-May Fu[e]

[a] Laboratory for Climate and Ocean-Atmosphere Studies, Department of Atmospheric and Oceanic Sciences, School of Physics, Peking University, Beijing, 100871, China
[b] Institute of Urban Meteorology, Beijing, 100089, China
[c] Multiphase Chemistry Department, Max Planck Institute for Chemistry, Mainz, 55128, Germany
[d] Laboratory for Earth Surface Processes, College of Urban and Environmental Sciences, Peking University, Beijing, 100871, China
[e] School of Environmental Science and Engineering, Southern University of Science and Technology, China

ARTICLE INFO

Keywords:
Ozone
Dry deposition
Planetary boundary layer
PBL parameterization

ABSTRACT

We present a regional modeling study that analyzes how planetary boundary layer (PBL) and surface layer parameterizations influence surface ozone concentrations and dry deposition fluxes over the Beijing-Tianjin-Hebei region in summer (July 2015). We use the Weather Research and Forecasting Model coupled to Chemistry (WRF-Chem) to simulate surface ozone concentration and dry deposition, and examine three PBL schemes: the Yonsei University (YSU), Mellor–Yamada–Janjić (MYJ), and Asymmetric Convective Model version 2 (ACM2) schemes. The model sensitivity to surface layer schemes is also tested by coupling the ACM2 PBL scheme with either the revised MM5-similarity scheme or the Pleim-Xiu surface layer scheme. Key physical and chemical factors for ozone dry deposition parameterization are analyzed to explore the root causes of model discrepancies. We find that all simulations overestimate the summertime daily mean ozone concentrations over North China (42 ppbv in observations vs. 43–50 ppbv in model results for July 2015) that are caused by high biases in daytime ozone and partly compensated by low biases in nighttime ozone. The YSU scheme has the largest overestimate in daily mean ozone concentration, but best reproduces the ozone diurnal cycle. The ACM2 scheme shows the largest underestimates of surface ozone over North China during nighttime, which can be explained by its weakest vertical mixing leading to high NO_x concentrations and strong ozone titration near surface. The choices of PBL and surface layer schemes lead to over 20% differences in ozone dry deposition fluxes due to differences in simulated surface ozone concentrations and dry deposition velocities. We find the differences in dry deposition velocity are mainly caused by differences in Monin-Obukhov length during nighttime and surface temperature during daytime. Our study emphasizes the needs to better understand these key PBL and surface factors for reducing the uncertainties in model simulation of surface ozone concentration and dry deposition.

1. Introduction

Ozone in the atmospheric planetary boundary layer (PBL) is an air pollutant that threatens human health and damages vegetation (Bates, 2005; Avnery et al., 2011). It also contributes to global warming as an important greenhouse gas (IPCC), and impacts the atmospheric oxidizing capability as a primary source of hydroxyl radical. The main source of tropospheric ozone is photochemical oxidation of volatile organic compounds (VOCs) and carbon monoxide in the presence of nitrogen oxides ($NO_x = NO + NO_2$). Human activities have significantly enhanced tropospheric ozone burden in the 20th century (Young et al., 2013; Cooper et al., 2014), which lead to 0.7 ± 0.3 million human death and 79–121 Tg of crop production reduction in 2000 (Anenberg et al., 2010; Avnery et al., 2011; Tai et al., 2014). In particular, the Beijing-Tianjin-Hebei (BTH) region in North China now suffers high levels of surface ozone pollution due to fast economic growth and industrial developments (Wang et al., 2006; Chan and Yao, 2008; Lu et al., 2018), and becomes a region with severe human health and

* Corresponding author.
E-mail address: zhanglg@pku.edu.cn (L. Zhang).
[1] Now at Laboratoire des Sciences du Climat et de l'Environnement, LSCE-IPSL (CEA-CNRS-UVSQ), Université Paris-Saclay, 91191 Gif-sur-Yvette, France.

https://doi.org/10.1016/j.atmosenv.2019.116950
Received 31 March 2019; Received in revised form 7 August 2019; Accepted 1 September 2019
Available online 06 September 2019

vegetation exposure to ozone pollution (Lu et al., 2018).

Removal of ozone in the PBL is mainly through chemical loss and dry deposition processes. On the global scale dry deposition removes about 25% of tropospheric ozone to the Earth's surface (Lelieveld and Dentener, 2000). Dry deposition velocities for ozone to vegetated areas are much higher than to non-vegetated areas, and vary with plant function types, leaf area index, and meteorological conditions (Wesely, 1989). Of all ozone deposited to the vegetated surface, one third to two thirds are usually taken up by plant stomata (Wesely and Hicks, 2000), representing a key pathway of ozone damage on plant health (Fowler et al., 2001). Other factors, such as land type, vegetation, and carbon dioxide concentrations, have also been found to directly or indirectly affect surface ozone concentration through dry deposition processes (Sitch et al., 2007; Fan et al., 2014; Tao et al., 2015; Heald and Geddes, 2016; Lai et al., 2016; Zhao et al., 2017; Zhang et al., 2017).

PBL meteorology heavily influences surface air quality in ways such as photochemistry, vertical mixing, and deposition (Garratt, 1994). The accuracy of air quality modeling then largely relies on the inputs of PBL meteorology from weather forecasting models. As the resolution of weather forecasting models usually cannot resolve the turbulent motions in the boundary layer, most of them apply PBL parameterizations to calculate the interplay of heat, moisture, and momentum between the sub-grid turbulence and large-scale advection. In the Weather Research and Forecasting model (WRF), a number of PBL parameterizations are implemented based on local or non-local closure schemes (Stull, 1988). Local closure schemes are developed based on the K-theory (e.g., the Mellor–Yamada–Janjić (MYJ) scheme, Janjić, 1990, 1994), in which turbulent mixing in each grid cell is only related to its adjacent layers. The local closure schemes are generally efficient for simulating stable PBL but underestimate vertical mixing by sub-grid large eddies under unstable PBL (Cohen et al., 2015). Non-local closure schemes often include a cross grid transport term to represent the large eddies (e.g., the Yonsei University (YSU) scheme, Hong et al., 2006). Although the non-local PBL schemes improve the representation of deep vertical mixing, they tend to deepen the PBL excessively (Cohen et al., 2015). There are also hybrid local-nonlocal PBL schemes such as the Asymmetric Convective Model v2 (ACM2) (Pleim, 2007), which apply local parameterizations for stable PBL and add non-local terms for unstable PBL.

Previous studies have evaluated WRF-Chem simulations of ozone concentrations using different PBL parameterizations in Houston (Cuchiara et al., 2014) and Mississippi Gulf coastal region (Yerramilli et al., 2010). Both studies demonstrated the importance of PBL parameterizations to surface ozone simulation. However, these work neither analyzed the reasons that led to model differences when using different PBL schemes, nor tested how PBL schemes influence estimates of ozone dry deposition as an important metric for vegetation exposure. In this study, we will investigate the sensitivities of surface ozone concentration and dry deposition to different PBL parameterizations using the WRF-Chem model with a focus on the BTH region. The aim of this study is not to choose a preferred PBL scheme in WRF-Chem, but to trace the root causes of model differences, and in particular to identify the key controlling PBL factors. Such analyses are important for pointing out factors that we need to improve in the PBL schemes for better simulating ozone pollution.

2. Method

2.1. The WRF-Chem model

We use the WRF-Chem v3.6 model (Grell et al., 2005) to investigate the sensitivity of surface ozone simulation to PBL parameterizations. Our analyses focus on July, a typical surface ozone peaking month. Each simulation is initialized on 27 June 2015 with the initial/boundary conditions of meteorology provided by NCEP Final Operational Global Analysis data (data available at http://rda.ucar.edu/datasets/ds083.2). The first 5 days are treated as spin-up and model results from 1 July 2015 are used for analysis. The 5-day spin-up is sufficient for the WRF-Chem regional model to initialize ozone conditions over BTH since ozone has a short lifetime of hours over high polluted regions (Monks et al., 2015). Meteorology is calculated online without applying the four-dimensional assimilation (FDDA) in the model. The model has a horizontal resolution of 27 km with 57 vertical layers from the surface to 10 hPa. As shown in Fig. 1, the model domain covers most of Eastern China and its adjacent oceans. The BTH region is surrounded by the Yan Mountains to the north and the Taihang Mountains to the west.

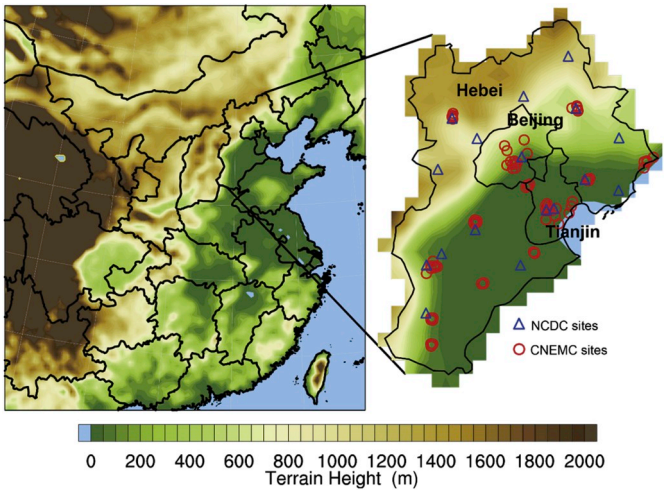

Fig. 1. Map of model domain (left panel) and the BTH region (right panel). Blue triangles denote the locations of NCDC meteorological sites and red circles denote CNEMC sites for surface ozone monitoring. (For interpretation of the references to colour in this figure legend, the reader is referred to the Web version of this article.)

Table 1 summarizes the model settings in this study. We use the Goddard Space Flight Center shortwave scheme (Chou and Suarez, 1994) and the rapid radiative transfer model (RRTM) (Mlawer et al., 1997) to simulate longwave and shortwave radiations, the single-moment 6-classes scheme and the Grell 3-D Cumulus scheme to parameterize cloud and precipitation (Grell and Dévényi, 2002), and the unified Noah land-surface model to estimate land surface properties. Chemical initial and boundary conditions are generated by the WRF-Chem preprocessor tool (MOZBC) from CAM-Chem outputs. The gas-phase chemistry is simulated by the Carbon Bound Mechanism version Z (CBMZ) with photolysis rates calculated by the Fast-J photolysis scheme. Aerosol formation is calculated by the Model for Simulating Aerosol Interactions and Chemistry (MOSAIC) with aerosol diameters divided into 4 size bins. Effects of aerosol on cloud formation (direct/indirect effects) are turned off (Zhou et al., 2019). Anthropogenic emissions are from the MIX emission inventory (Li et al., 2017) for 2015 over East Asia. Natural emissions include Fire INventroy from NCAR

Table 1
WRF-Chem model configurations.

Meteorology initial/boundary conditions	FNL analysis and forecast every 6 h
Chemistry initial/boundary conditions	MOZBC
Land surface	Noah
Shortwave radiation	Goddard Space Flight Center
Longwave radiation	RRTM
Cumulus parameterization	Grell 3-D scheme
Microphysics	Single-moment 6-class scheme
Gas-phase chemistry	CBMZ
Aerosol scheme	MOSAIC (4 bins)
Photolysis scheme	Fast-J

(FINN; data available at http://bai.acom.ucar.edu/Data/fire/) and biogenic VOC emissions calculated by the Model of Emissions of Gases and Aerosols from Nature (MEGAN) (Guenther et al., 2012).

2.2. Dry deposition calculation in WRF-Chem

Dry deposition fluxes (F_d) in WRF-Chem are calculated as the product of tracer concentration and dry deposition velocity (v_d) at the lowest model layer (z_1). Based on the resistance-in-series model (Wesely, 1989), v_d is parameterized as:

$$v_d = 1/(R_a + R_b + R_c) \quad (1)$$

where R_a is the aerodynamic resistance to the transfer from z_1 to the roughness height (z_o). Based on the similarity theory, R_a largely depends on the surface layer stability and is calculated as a function of surface layer turbulence parameters including friction velocity (u*) and the Monin-Obukhov length (L):

$$R_a(z_1, z_o) = \int_{z_c}^{z_1} \Phi\left(\frac{z}{L}\right)/\left(ku^*\frac{z}{L}\right)d\frac{z}{L} \quad (2)$$

Here Φ is a stability-dependent function (Businger et al., 1971) and k is the von Karman constant. Generally, R_a values are much larger in stable boundary mixing layers than those in unstable boundary mixing layers. R_b is the boundary layer resistance to transfer between the roughness height and the actual surface. R_c is the resistance to surface uptake, which can be further divided into several series and parallel components to represent resistances to vegetation, the lower canopy, and ground. Among the resistances, R_b is typically much smaller than R_a and R_c, and is often neglected in many models. For ozone dry deposition calculations in WRF-Chem, R_b is set to be a small constant for a given land type, and is thus not discussed in this study.

Model parameterizations of PBL mixing can influence the calculation of R_a by affecting the PBL parameters, such as friction velocity and Monin-Obukhov length in Eq. (2), and also influence R_c by affecting model simulation of meteorological parameters at surface. The R_c is calculated by the Ohm's law:

$$R_c = \left(\frac{1}{R_s + R_m} + \frac{1}{R_{lu}} + \frac{1}{R_{dc} + R_{cl}} + \frac{1}{R_g}\right)^{-1} \quad (3)$$

Here the bulk resistances to leaf stomata (R_s), to the leaf mesophyll (R_m), to the upper canopy (R_{lu}), to the buoyant transfer of gases over the lower canopy (R_{dc}), to surface in the lower canopy (R_{cl}), and to the ground (R_g) are considered. Although R_c includes several components as shown above, for ozone, only the bulk resistance to leaf stomata R_s and the resistance to buoyant transfer of gases over the lower canopy R_{dc} are parameterized to be affected by meteorological conditions including solar radiation reaching ground (GSW) and surface temperature (T_s) using the equations below:

$$R_s = R_i\{1 + [200(\mathrm{GSW}+0.1)^{-1}]^2\}\{400[T_s(40 - T_s)]^{-1}\} \quad (4)$$

$$R_{dc} = 100[1 + 1000(\mathrm{GSW}+10)^{-1}](1 + 1000\theta)^{-1} \quad (5)$$

where R_i is a constant given for each season and θ is the slope of local terrain. When surface temperature is outside the range of 0–40 °C, R_s values would then become very large as the leaf stomata close under too cold or too warm conditions. R_s can also be influenced by humidity and soil moisture (Noilhan and Planton, 1989; Anav et al., 2018), but is not considered in the Wesely scheme.

2.3. Model experiments

We design four model experiments to investigate the sensitivity of ozone simulation to PBL parameterizations as listed in Table 2. Three PBL parameterizations are employed, including the local closure MYJ scheme (Janjić, 1990, 1994), non-local closure YSU scheme (Hong et al., 2006), and hybrid local-nonlocal ACM2 scheme (Pleim, 2007), to account for different turbulence closures. Each PBL scheme is coupled to a specified surface layer (SFL) scheme, which calculates exchanges of heat, moisture and momentum between the land surface and the PBL. The YSU scheme can only be applied with the revised MM5-similarity SFL scheme (Zhang and Anthes, 1982), while MYJ is coupled to the Eta-similarity SFL scheme (Janjic, 1996). The ACM2 scheme can be applied with either the revised MM5-similarity scheme or the Pleim-Xiu SFL scheme (Pleim, 2006; Gilliam and Pleim, 2009).

Table 2
List of model experiments.

Simulation	PBL scheme	Surface layer scheme
YSU_MM5	YSU	Revised MM5
MYJ_Eta	MYJ	Eta similarity
ACM2_MM5	ACM2	Revised MM5
ACM2_PX	ACM2	Pleim-Xiu

Generally, the SFL parameterizations estimate the land-PBL exchanges by solving the flux–profile relationships with the similarity theory. The revised-MM5 scheme calculates the similarity functions for four different stability regimes defined by the bulk Richardson number (Zhang and Anthes, 1982), while the Pleim-Xiu SFL scheme only separates stable and unstable conditions (Pleim, 2006). The Eta-similarity scheme applies the Beljaars (1995) correction for the free convention cases. The thermal roughness length parameterization, which corrects the inconsistency lead by using potential temperature at ground as boundary conditions, is only implied in the Pleim-Xiu SFL and Eta-similarity schemes (Janjic, 1996; Pleim, 2006).

Here we use the model simulation with the YSU PBL scheme and the revised MM5 SFL scheme (YSU_MM5) as the base simulation. Simulated differences in sensitivity simulations (MYJ_Eta and ACM2_MM5) relative to the base simulation then represent the overall influences from PBL and SFL schemes. We also examine the model sensitivity to SFL parameterizations alone using the ACM2_PX simulation (the ACM2 PBL scheme coupled to the Pleim-Xiu SFL scheme).

We compare the WRF-Chem simulated meteorological fields using different PBL parameterizations with measurements from the National Climate Data Center (NCDC; https://gis.ncdc.noaa.gov/maps/ncei/cdo/hourly) database. Fig. 1 shows the locations of NCDC sites over the BTH region, and Fig. 2 presents the time series of observed vs. simulated meteorological variables including surface 2-m temperature, dew point temperature, and 10-m wind speed for July 2015 averaged over the BTH sites. The correlation coefficient and the normalized mean bias (Bias = $\sum_{i=1}^{N}(M_i - O_i)/\sum_{i=1}^{N} O_i$) for N observed (O) and model (M) values are calculated as statistical metrics. Supplementary Fig. S1 shows observed vs. modeled diurnal variations with the root-mean-square error (RMSE = $\sqrt{\frac{1}{N}\sum_{i=1}^{N}(M_i - O_i)^2}/\sum_{i=1}^{N} O_i$) calculated. As shown in Fig. 2 and Fig. S1, all model simulations generally capture observed surface temperature and dew point temperature (humidity) with small mean biases and RMSE of less than 1%, but they all tend to overestimate surface wind speed by more than 30%. Even larger biases (generally over 80%) can be seen when comparing the zonal and meridional wind components (Supplementary Fig. S2). The high biases in wind speed may be caused by several factors such as coarse model resolution (Wang et al., 2016) and not well representation of urban heat island (Fan et al., 2013). Such bias can be partly corrected with nested grids (Wang et al., 2016). Model evaluations of meteorology also indicate that PBL parameterizations have small influenes on the simulated monthly mean meteorological variables over BTH, similar to a previous study focused on Houston in the US (Cuchiara et al., 2014). However, the differences can be episodically significant, in particular for wind speed (Fig. 2 and Fig. S2).

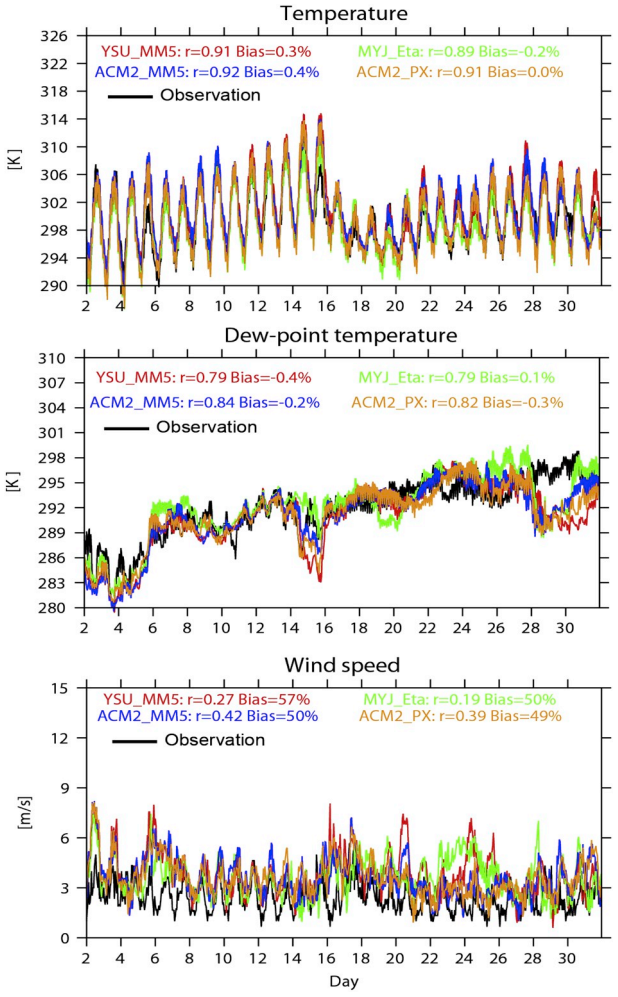

Fig. 2. Measured and simulated hourly 2m temperature (top), dew-point temperature (middle), and wind speed (bottom) averaged over the BTH NCDC sites in July 2015. Measurements (black lines) are compared with model results from YSU_MM5 (red), MYJ_Eta (green), ACM2_MM5 (blue), and ACM2_PL (yellow) sampled at the BTH NCDC sites. (For interpretation of the references to colour in this figure legend, the reader is referred to the Web version of this article.)

3. Results

3.1. Influences of PBL scheme on ozone concentration

We evaluate the model simulation of ozone concentrations using surface measurements from the China National Environmental Monitoring Center (CNEMC) Network (http://113.108.142.147:20035/emcpublish/). Fig. 1 also shows the locations of the CNMEC sites. Fig. 3 shows the measured and simulated surface ozone diurnal cycles averaged over the CNMEC sites in BTH. All model simulations, while capturing the strong ozone diurnal cycle, overestimate the observed mean ozone concentration in July 2015 over BTH by 1–8 ppbv (42.1 ppbv in observations vs. 43.2–50.5 ppbv in model results). When comparing hourly surface ozone values, we can see that the mean biases are caused by large overestimates in daytime ozone (over 20 ppbv at noon) and are partly offset by underestimates during nighttime. Previous studies have pointed out that underestimation of nighttime ozone by WRF-Chem may due to uncertainties in ozone and NO reactions (Chen et al., 2013; Žabkar et al., 2015). Comparisons with hourly surface NO_2 measurements show large model overestimates during nighttime (Fig. S3). All model results simulate the daily ozone peak time about 2 h earlier than measurements, reflecting model biases in the NO_x emission diurnal cycle or the chemical mechanism. The model simulation with the ACM2

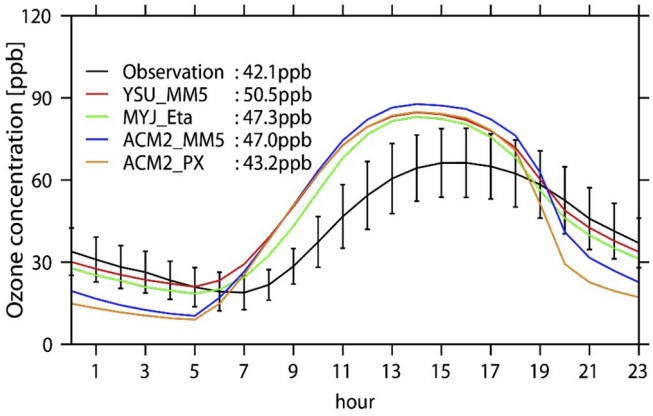

Fig. 3. Mean diurnal cycle of surface ozone concentrations in July 2015 averaged over the BTH MEP sites (Fig. 1). The black line represents the averages of MEP observations with vertical bars denoting the standard deviations among sites. Colored lines are corresponding model results with different PBL schemes.

scheme shows much larger underestimation (~10 ppbv lower) than model results with YSU and MYJ schemes during nighttime. This is consistent with Cuchiara et al. (2014) that also found simulations of surface ozone concentrations at Houston with ACM2 are distinctly different from those with other PBL schemes. We find here that although the YSU scheme has the largest bias in daily mean ozone, it shows relatively better agreement with the measured diurnal cycle as indicated by the smaller model underestimates (< 4 ppbv) during nighttime.

To further understand model simulated differences due to different PBL schemes, we compare in Fig. 4 the diurnal variations of ozone and NO_2 vertical profiles in the lowest 1 km as simulated by YSU_MM5 and ACM2_MM5. Here and afterwards, the model results are averaged over the whole BTH grids to better represent this region. During nighttime (2000-0700 local time), ACM2_MM5 simulates lower ozone

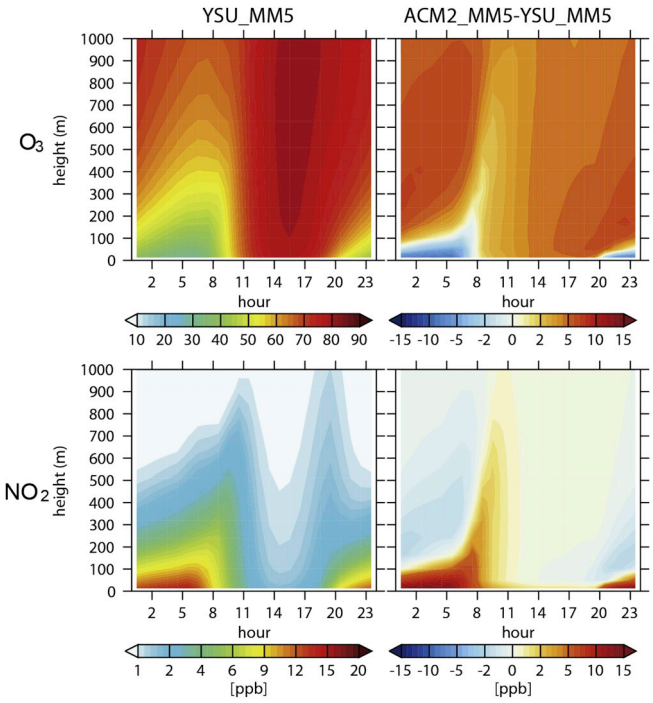

Fig. 4. Diurnal cycles of ozone (top panels) and NO_2 (bottom panels) vertical profiles in the lowest 1 km in July 2015. Model results of YSU_MM5 (left panels) are compared with ACM2_MM5 calculated as ACM2_MM5 minus YSU_MM5 in the right panels.

concentrations than YSU_MM5 near surface (below 100m) but higher ozone concentrations at higher altitudes above 100 m. During daytime (0800–1900 local time), ACM2_MM5 generally simulates higher ozone concentrations throughout the lowest 1 km. Both ozone and NO_2 levels show distinct vertical gradients during nighttime (2000-0700 local time) when PBL is stable. As all emissions of nitric oxide (NO) are emitted in the lowest model layer in this study, near-surface NO_2 concentrations are highly sensitive to vertical mixing. We attribute the differences between YSU_MM5 and ACM2_MM5 to the weaker vertical mixing under nighttime stable boundary layers calculated by the ACM2 PBL scheme. Weaker vertical mixing during nighttime in ACM2_MM5 than other PBL schemes leads to more NO (Fig. S4) and NO_2 and thus stronger ozone titration near surface. Lower NO_2 concentrations and less ozone mixed to the surface together lead to higher ozone concentrations at higher altitudes (above 100m) in ACM2_MM5. During the daytime, strong vertical mixing under unstable boundary layers can then mix the more preserved NO_2 to high altitudes and lead to higher ozone formation in ACM2_MM5.

One important uncertainty in the discussion above can be the vertical placement of emissions in the model. NO_x emissions from power plant and industry chimneys, which account for 65% of total NO_x emissions over the BTH region, are elevated point sources. For example, heights of chimneys of electrical generating units are usually 100–238m (Song et al., 2006), corresponding to the 3rd–5th levels in our model simulation. Assuming all NO_x is emitted in the lowest model layer (0–25m) may affect the WRF-Chem ozone simulation and its sensitivity to PBL schemes. Here we have further performed additional model experiments for YSU_MM5 (YSU_MM5_2) and ACM2_MM5 (ACM2_MM5_2) but using elevated NO_x sources from power plant and industry following Table S1. It should be noted that these simulations still may not fully represent the vertical distributions of NO_x emissions due to a lack of such information in the Chinese emission inventory and not considering plume rise (Guevara et al., 2014) as well. As shown in Supplementary Fig. S5, model results with elevated NO_x sources would largely improve the model nighttime ozone simulation. Model underestimates of nighttime ozone levels in ACM2_MM5 decrease from about 20 ppbv to less than 10 ppbv, and model results with YSU_MM5 show near zero bias during nighttime. However, changing emissions height leads to minor changes in daytime surface ozone concentrations due to strong vertical mixing under unstable PBL conditions. Previous studies have found that changes in NO_x emission intensity affected nighttime surface ozone concentrations (Awang et al., 2015; Yan et al., 2018). Here we show that vertical distributions of NO_x emissions from elevated point sources can be also an important factor. The simulated differences between ACM_MM5 and YSU_MM5 largely remain, reflecting the impacts of PBL parameterization as discussed above.

3.2. Influences on ozone dry deposition

We now examine how PBL schemes influence ozone dry deposition as simulated by the WRF-Chem model. Fig. 5 shows the spatial distribution of ozone dry deposition fluxes simulated by YSU_MM5 averaged over daytime and nighttime of July 2015, and the differences between YSU_MM5 and other PBL schemes. Ozone dry deposition fluxes are higher to the northern part of BTH (over 2.6 $kg\,km^{-2}\,h^{-1}$ for the daytime mean and 1.2 $kg\,km^{-2}\,h^{-1}$ for the nighttime mean) than the southern part (1.0–1.2 $kg\,km^{-2}\,h^{-1}$ for the daytime mean and 0.6–1.0 $kg\,km^{-2}\,h^{-1}$ for the nighttime mean). Higher dry deposition fluxes to the northern BTH are mainly driven by higher dry deposition velocities in the daytime, and by both higher ozone concentrations (Fig. S6) and dry deposition velocities in the nighttime. As for the total ozone dry deposition to BTH, daytime mean fluxes (2.0×10^8 $kg\,month^{-1}$) are more than twice as nighttime values (0.92×10^8 $kg\,month^{-1}$). YSU_MM5 simulates the lowest dry deposition fluxes during daytime (about 20% lower than MYJ_Eta and ACM2_PX at noon), but more than 30% higher than ACM2_PX at night.

Fig. 6 shows diurnal variations of simulated ozone dry deposition fluxes averaged over BTH using the YSU_MM5 scheme. We also analyze here the differences in surface ozone concentration, ozone dry deposition velocity and flux when using other PBL schemes. We can see that both differences in surface ozone concentration and dry deposition velocity lead to model simulated differences in ozone dry deposition fluxes, and the latter shows a larger contribution. As shown in Fig. 6, nighttime ozone dry deposition velocities and surface ozone concentrations in ACM2_PX are, respectively, 0.05–0.1 $cm\,s^{-1}$ (15–30%) and 5–15 ppbv (5–35%) lower than YSU_MM5, resulting in 0.2–0.4 $kg\,km^{-2}\,h^{-1}$ (8–35%) lower dry deposition fluxes. Higher daytime ozone dry deposition fluxes simulated by MYJ_Eta and ACM2_PX are mainly caused by higher dry deposition velocities (more than 0.1 $cm\,s^{-1}$), while higher daytime fluxes in ACM2_MM5 than YSU_MM5 are caused by higher surface ozone concentrations. The comparison of ACM2_MM5 and ACM2_PX model results indicate that calculations of dry deposition velocity are sensitive to surface layer parameterization.

Hardacre et al. (2015) previously compared simulated ozone dry deposition fluxes by 15 chemical transport models that contributed to the TF HTAP model inter-comparison project, and found inter-model differences of over 0.1 $cm\,s^{-1}$ in dry deposition velocity and about 20% in ozone dry deposition flux over the Northern Hemisphere. They pointed out that improving dry deposition velocities is essential for better simulating ozone dry deposition fluxes. Our model experiments find that different PBL and surface schemes can lead to such large discrepancies in model estimates of ozone dry deposition velocity and flux.

3.3. Key factors affecting ozone dry deposition

We further diagnose the key factors that influence ozone dry deposition velocities over BTH for the summer month of July 2015. As described in Sect. 2.2, the calculation of dry deposition velocity depends on estimates of aerodynamic resistance (R_a) and surface resistance (R_c). Fig. 7 and Fig. 8, respectively, examine the model simulated differences in R_a and R_c as resulted from different PBL and surface schemes and their driving factors. Both R_a and R_c show larger values during nighttime (80 $s\,m^{-1}$ for R_a and 250 $s\,m^{-1}$ for R_c) than daytime values (50 $s\,m^{-1}$ for R_a and 150 $s\,m^{-1}$ for R_c) in YSU_MM5 due to stable PBL and zero solar radiation at night. R_c is about a factor of 3 larger than R_a through the day in YSU_MM5, but the MYJ_Eta and ACM2_PX schemes estimate higher or comparable R_a relative to R_c at night. We can see that model differences in dry deposition velocity using different PBL/SFL schemes are mainly driven by differences in R_a during nighttime and in R_c during daytime.

During nighttime, stable PBL conditions are associated with small friction velocity (u*) and positive Monin-Obukhov length (L). As shown in Fig. 7, R_a values are highly sensitive to the inverse of the Monin-Obukhov length, which reflects the stability of the PBL. Smaller positive L (larger 1/L) values correspond to more stable PBL and thus larger R_a. Compared to YSU_MM5, MYJ_Eta simulates very stable PBL with average 1/L occasionally greater than 0.2 (more than 5 times larger than YSU_MM5) at night, leading to extremely high R_a values (> 300 $s\,m^{-1}$). ACM2_PX simulates more stable PBL (mean 1/L of ~0.1 during nighttime) over the whole BTH region, resulting in larger R_a (~100 $s\,m^{-1}$) and smaller dry deposition velocities. Using the same surface layer scheme, ACM2_MM5 generally simulates similar R_a values as YSU_MM5.

During daytime, R_c values simulated by MYJ_Eta and ACM2_PX are about 20% lower than those by YSU_MM5 and ACM2_MM5. Based on Equations (4) and (5), R_c values decrease with increasing ground-level downward shortwave radiation (GSW), and increase when surface temperature deviates from 20 °C. The MYJ_Eta and ACM2_PX schemes simulate lower GSW by about 50 $W\,m^{-2}$ and lower surface temperature by about 6 °C than YSU_MM5 and ACM2_MM5. Although lower GSW

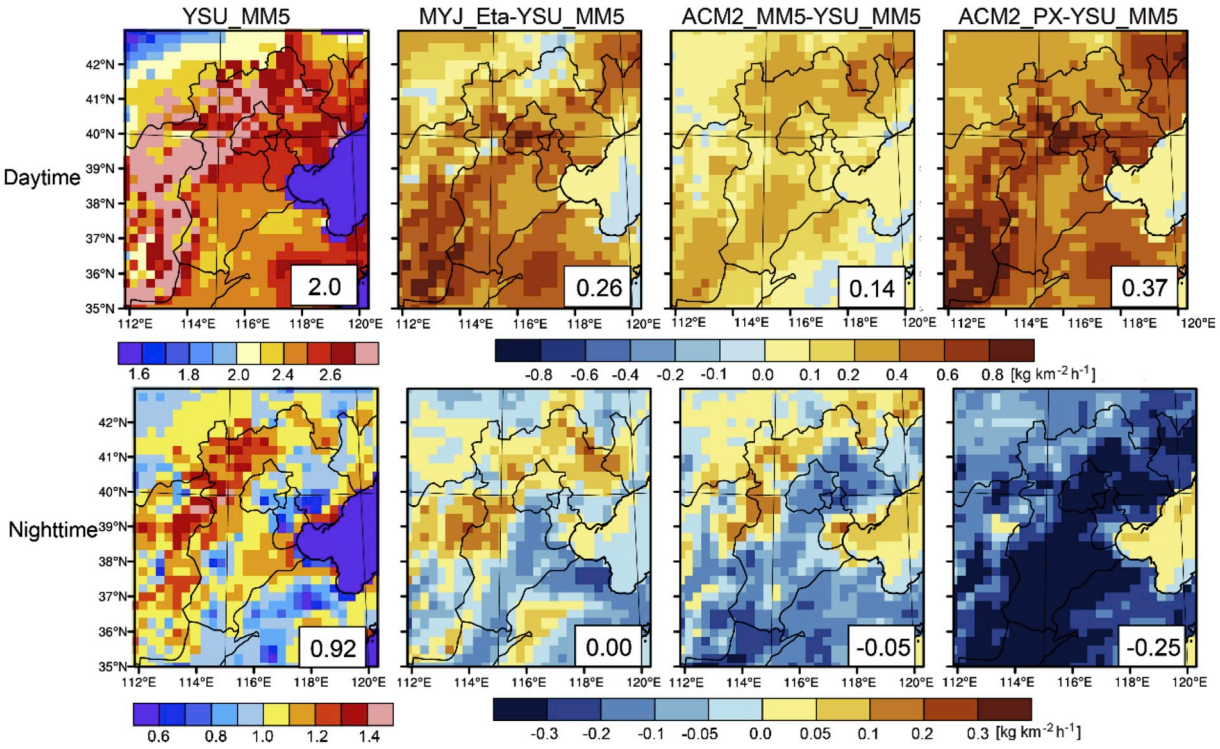

Fig. 5. Spatial distributions of daytime (0800–1900 local time; top row) and nighttime (2000-0700 local time; bottom row) mean ozone dry deposition fluxes simulated in YSU_MM5 (first column), and their differences between YSU_MM5 and other sensitivity simulations (second to fourth columns). Total deposition values to BTH (in unit of 10^8 kg month^{-1}) are shown inset.

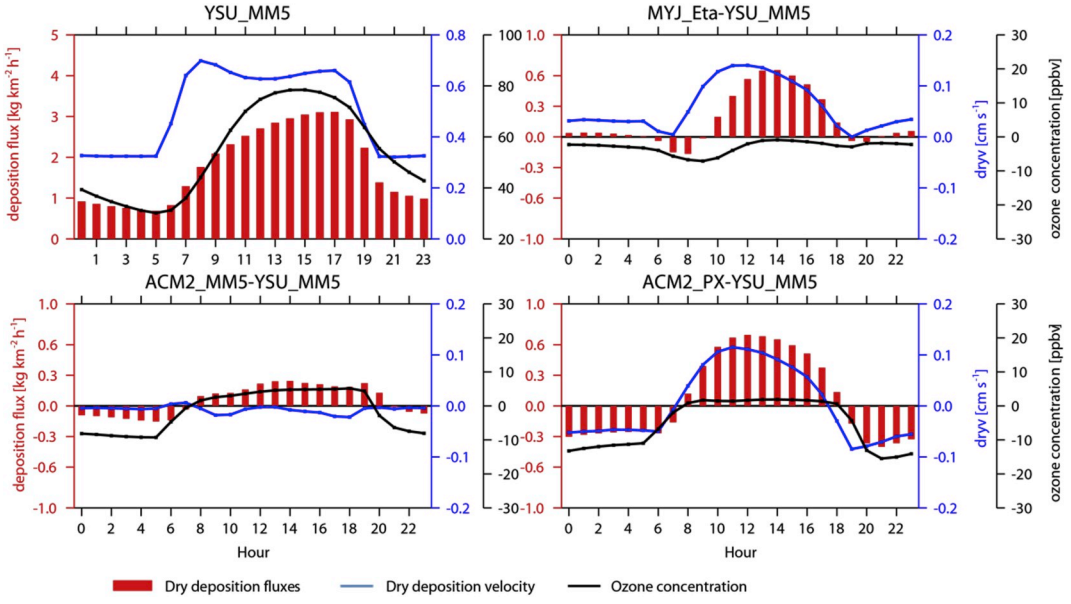

Fig. 6. Diurnal cycles of hourly ozone dry deposition fluxes (red bars), surface ozone concentrations (black lines), and dry deposition velocities (blue lines) in July 2015 averaged over BTH. The top left panel shows model results from YSU_MM5, and the other three panels show simulated differences by MYJ_Eta (top right), ACM2_MM5 (bottom left), and ACM2_PX (bottom left) relative to YSU-MM5. (For interpretation of the references to colour in this figure legend, the reader is referred to the Web version of this article.)

would enhance R_c, lower surface temperature lead to large R_c decreases, resulting in smaller R_c by about 25 s m^{-1} in MYJ_Eta and ACM2_PX relative to YSU_MM5. Surface temperature is thus a key factor driving the differences in daytime R_c calculation. Similar to R_a at night, daytime R_c values in YSU_MM5 and ACM2_MM5 show small differences. We also find the R_a and R_c differences simulated by different PBL and surface layer schemes are not sensitive to land cover types. Compared with averages of the whole BTH region as shown in Figs. 6–8, averages over different land cover types (e.g., crop land, grass land, and broadleaf forest) in this region show similar results (Supplementary Figs. S7–S9).

We can further explain the model simulated differences in surface temperature over the BTH region by analyzing the energy budget following the approach of Xie et al. (2012). In the absence of rain and snow, the energy balance equation can be written as:

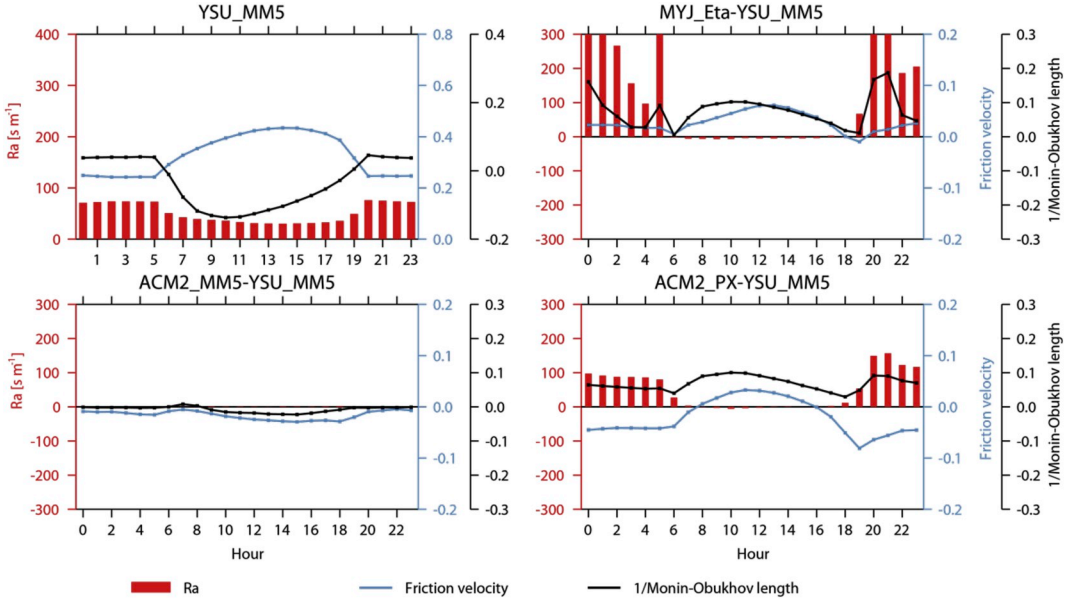

Fig. 7. Same as Fig. 6, but for aerodynamic resistance R_a (red bars), friction velocity (blue lines), and inverse of the Monin-Obukhov length (black lines). (For interpretation of the references to colour in this figure legend, the reader is referred to the Web version of this article.)

$$GSW + GLW - (LH+SH + GRDFLX + \varepsilon\sigma T^4) = 0 \quad (6)$$

where GLW is net downward longwave radiation, LH and SH are latent heat and sensible heat fluxes, GRDFLX is the ground heat flux, and $\varepsilon\sigma T^4$ is surface upward longwave radiation that can be used to diagnose surface temperature (T). As shown in Fig. 9, YSU_MM5 simulates higher GSW values (by up to 50 W m^{-2}) than MYJ_Eta, ACM2_MM5, and ACM2_PX, which are mainly due to lower cloud coverage and density in YSU_MM5 (Xie et al., 2012). The differences in cloud reflect the coupling of sub-grid meteorological variables simulated by different PBL schemes with the cloud microphysics (Xie et al., 2012), and less cloud simulated by YSU than MYJ is likely due to smaller equipotential temperature increases during daytime in YSU (Milovac et al. (2016)). Compared with YSU_MM5, ACM2_MM5 simulates lower GSW values but are offset by lower surface LH, leading to similar surface temperature and R_c simulations. The MYJ_Eta and ACM2_PX schemes, however, emit more LH and SH during daytime, and together decrease the surface upward longwave radiation (i.e., $\varepsilon\sigma T^4$ or the net radiation in Fig. 9) by up to 50 W m^{-2} at noon, which explains the lower surface temperature and thus R_c compared with YSU_MM5. As LH/SH is calculated in the model surface layer scheme as functions of exchange coefficients for moisture/heat and near-surface moisture/potential temperature gradients, this also reflects the impact of the surface layer parameterization on model simulation of ozone dry deposition.

4. Conclusions and discussion

In summary, we have conducted a regional modeling study to investigate the sensitivity of summertime surface ozone concentrations and dry deposition fluxes to different PBL and surface layer parameterizations over the BTH region, and to further explore the root

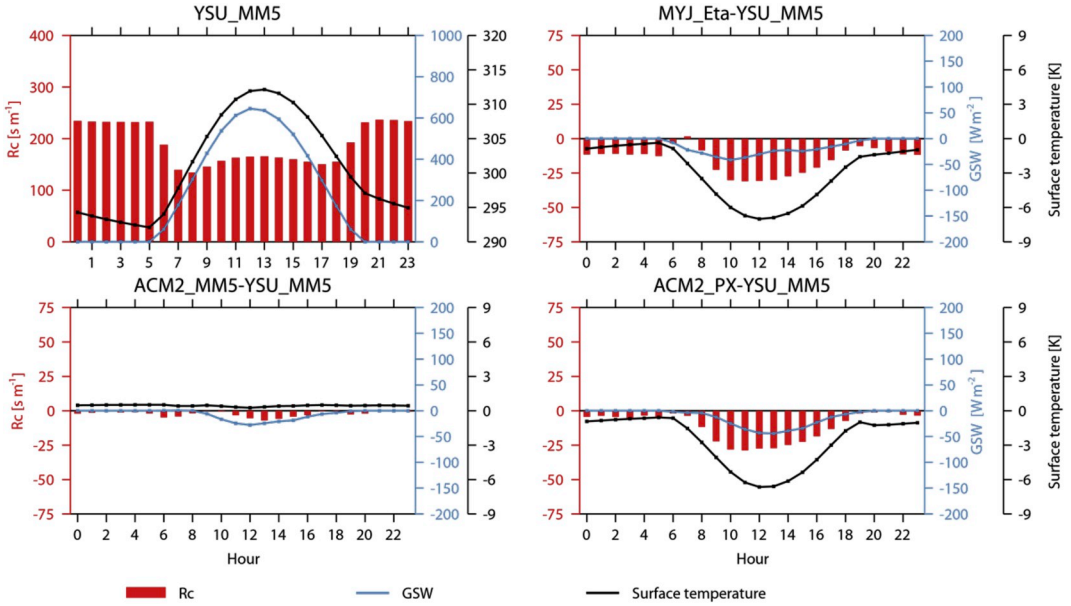

Fig. 8. Same as Fig. 6, but for surface resistance R_c (red bars), ground-level shortwave radiation (GSW; blue lines), and surface temperature (black lines). (For interpretation of the references to colour in this figure legend, the reader is referred to the Web version of this article.)

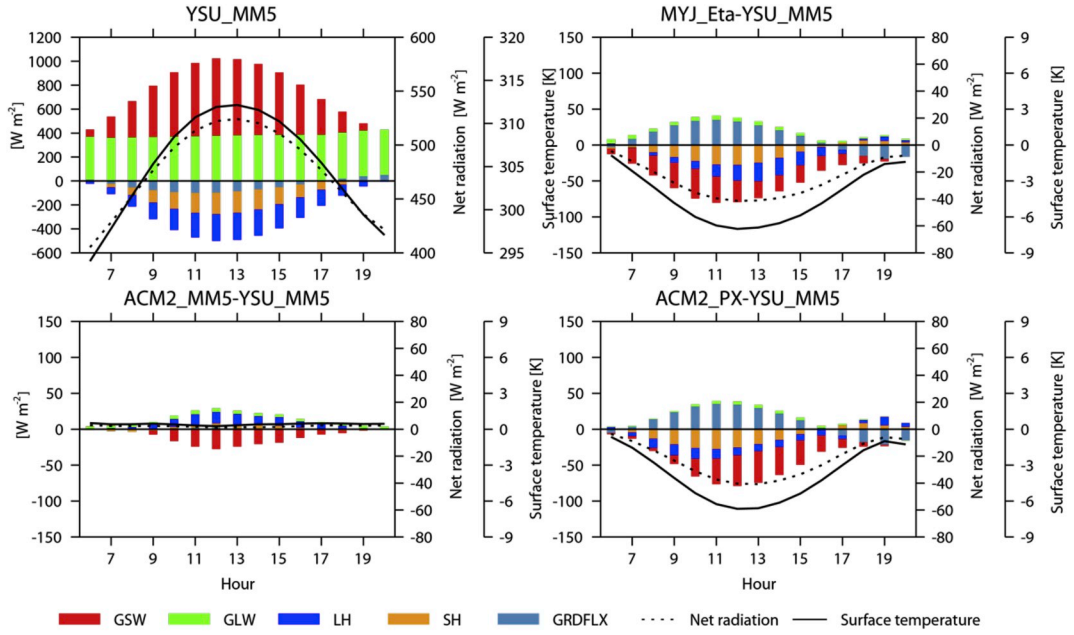

Fig. 9. Hourly surface energy flux budget averaged over BTH during 0600–2000 local time in July 2015. The top left panel shows model results from YSU_MM5 and the other three panels show differences in sensitivity simulations with different PBL and surface layer schemes relative to YSU_MM5. Net shortwave and longwave radiation reaching the ground (GSW and GLW), latent heat fluxes (LH), sensible heat fluxes (SH), and ground heat fluxes (GRDFLX) are shown by histograms. Their net fluxes represent longwave radiation emitted by the ground (dash lines). Also shown are model results of surface temperature (solid lines).

causes of model differences. We conduct the WRF-Chem model simulations with three PBL schemes representing different turbulence closures including YSU (local), MYJ (non-local) and ACM2 (hybrid). The YSU and MYJ schemes are, respectively, coupled to MM5-similarity and Eta-similarity surface layer schemes, while the ACM2 scheme can be applied with both MM5-similarity and Pleim-Xiu schemes allowing us to further test the influence from surface layer parameterizations. Model simulated 2-m temperature, humidity, and wind speed are evaluated with observations over BTH, and all show reasonable agreements. Simulated meteorological variables using different PBL schemes, although have small differences in the monthly means, may differ considerably occasionally.

PBL schemes moderately influence model simulation of surface ozone diurnal cycles and show large impacts on ozone dry deposition fluxes. Evaluated by in situ observations, model simulations with all PBL schemes show similar overestimates of surface ozone concentrations during daytime, but simulations with the ACM2 scheme show much larger underestimates of 10 ppbv than YSU and MYJ at night. The lower nighttime surface ozone simulated by ACM2 than other schemes can be explained by its weaker vertical mixing, which leads to stronger NO_2 concentrations and ozone titration near surface. Additional sensitivity experiments with point NO_x sources emitted at higher model layers can largely reduce the model nighttime ozone underestimates, which indicates that both PBL mixing strength and vertical NO_x emission distributions are crucial for better simulating nighttime ozone concentrations.

Using different PBL and surface schemes, the WRF-Chem simulated ozone dry deposition fluxes differ from each other by over 20% during daytime and 30% during nighttime. These discrepancies reflect combined impacts of differences in surface ozone concentrations and dry deposition velocities. By analyzing aerodynamic resistance (R_a) and surface resistance (R_c) separately, we conclude that the key factors influencing WRF-Chem model simulation of ozone dry deposition velocity are the Monin-Obukhov length for R_a, which reflecting the stability of the surface layer during nighttime, and surface temperature for R_c, which is determined by ground radiation balance during daytime. This finding points out the importance of improving PBL and surface layer parameterizations for better simulating dry deposition fluxes of atmospheric composition and understanding their environmental consequences via biosphere-atmosphere interactions.

The above analyses of influences of PBL parameterization on ozone dry deposition are based on the commonly used Wesely scheme (Wesely, 1989), which applies a uniform “big-leaf” model to simplify the canopy structures. There are other dry deposition schemes that consider more complex canopy structures such as the two-big-leaf model (Zhang et al., 2002, 2003), ecological processes including plant photosynthesis (Wu et al., 2012) and soil moisture impacts on stomal conductance (Noilhan and Planton, 1989; Anav et al., 2018), and coupling with land surface model (Pleim et al., 2001). For example, Park et al. (2014) found that ozone dry deposition velocities over East Asia estimated by the Wesely scheme can be 0.24 cm s^{-1} higher than those by the M3DRY scheme (Pleim et al., 2001). Responses of ozone dry deposition to PBL parameterizations can also vary with dry deposition schemes. In addition, Rc is linked to land surface properties including temperature, moisture, and heat fluxes, and is thus strongly influenced by land surface models. Future work is required to better understand the influences of land surface models and dry deposition parameterizations on dry deposition modeling and associated uncertainties.

Declaration of competing interest

The authors declare that they have no known competing financial interests or personal relationships that could have appeared to influence the work reported in this paper.

Acknowledgements

This work is supported by the National Key Research and Development Program of China (2017YFC0210102) and the Beijing Municipal Science and Technology Project (Z181100005418016).

Appendix A. Supplementary data

Supplementary data to this article can be found online at https://doi.org/10.1016/j.atmosenv.2019.116950.

References

Anav, A., Proietti, C., Menut, L., Carnicelli, S., De Marco, A., Paoletti, E., 2018. Sensitivity of stomatal conductance to soil moisture: implications for tropospheric ozone. Atmos. Chem. Phys. 18, 5747–5763.

Anenberg, S.C., Horowitz, L.W., Tong, D.Q., West, J.J., 2010. An estimate of the global burden of anthropogenic ozone and fine particulate matter on premature human mortality using atmospheric modeling. Environ. Health Perspect. 118, 1189–1195.

Avnery, S., Mauzerall, D.L., Liu, J., Horowitz, L.W., 2011. Global crop yield reductions due to surface ozone exposure: 1. Year 2000 crop production losses and economic damage. Atmos. Environ. 45, 2284–2296.

Awang, N.R., Ramli, N.A., Yahaya, A.S., Elbayoumi, M., 2015. High nighttime ground-level ozone concentrations in Kemaman: NO and NO_2 concentrations attributions. Aerosol. Air Qual. Res. 15, 1357–1366.

Bates, D.V., 2005. Ambient ozone and mortality. Epidemiology 16, 427–429.

Beljaars, A.C., 1995. The parametrization of surface fluxes in large-scale models under free convection. Q. J. R. Meteorol. Soc. 121, 255–270.

Businger, J.A., Wyngaard, J.C., Izumi, Y., Bradley, E.F., 1971. Flux-profile relationships in the atmospheric surface layer. J. Atmos. Sci. 28, 181–189.

Chan, C.K., Yao, X., 2008. Air pollution in mega cities in China. Atmos. Environ. 42, 1–42.

Chen, D., Li, Q., Stutz, J., Mao, Y., Zhang, L., Pikelnaya, O., Tsai, J.Y., Haman, C., Lefer, B., Rappenglück, B., Alvarez, S.L., Neuman, J.A., Flynn, J., Roberts, J.M., Nowak, J.B., de Gouw, J., Holloway, J., Wagner, N.L., Veres, P., Brown, S.S., Ryerson, T.B., Warneke, C., Pollack, I.B., 2013. WRF-Chem simulation of NO_x and O_3 in the L.A. basin during CalNex-2010. Atmos. Environ. 81, 421–432.

Chou, M.-D., Suarez, M.J., 1994. An efficient thermal infrared radiation parameterization for use in general circulation models. NASA Technical Memorandum No. 104606 3.

Cohen, A.E., Cavallo, S.M., Coniglio, M.C., Brooks, H.E., 2015. A review of planetary boundary layer parameterization schemes and their sensitivity in simulating southeastern U.S. Cold season severe weather environments. Weather Forecast. 30, 591–612.

Cooper, O.R., Parrish, D., Ziemke, J., Cupeiro, M., Galbally, I., Gilge, S., Horowitz, L., Jensen, N., Lamarque, J.-F., Naik, V., 2014. Global distribution and trends of tropospheric ozone: an observation-based review. Elem Sci Anth 2, 000029.

Cuchiara, G.C., Li, X., Carvalho, J., Rappenglück, B., 2014. Intercomparison of planetary boundary layer parameterization and its impacts on surface ozone concentration in the WRF/Chem model for a case study in Houston/Texas. Atmos. Environ. 96, 175–185.

Fan, Q., Liu, Y., Wang, X., Fan, S., Chan, P.W., Lan, J., Feng, Y., 2013. Effect of different meteorological fields on the regional air quality modelling over Pearl River Delta, China. Int. J. Environ. Pollut. 53, 3–23.

Fan, Q., Yu, W., Fan, S., Wang, X., Lan, J., Zou, D., Feng, Y., Chan, P.-W., 2014. Process analysis of a regional air pollution episode over Pearl River Delta Region, China, using the MM5-CMAQ model. J. Air Waste Manag. Assoc. 64, 406–418.

Fowler, D., Flechard, C., Cape, J.N., Storeton-West, R.L., Coyle, M., 2001. Measurements of ozone deposition to vegetation quantifying the flux, the stomatal and non-stomatal components. Water Air Soil Pollut. 130, 63–74.

Garratt, J.R., 1994. Review: the atmospheric boundary layer. Earth Sci. Rev. 37, 89–134.

Gilliam, R.C., Pleim, J.E., 2009. Performance assessment of new land surface and planetary boundary layer physics in the WRF-ARW. J. Appl. Meteorol. Climatol. 49, 760–774.

Grell, G.A., Dévényi, D., 2002. A generalized approach to parameterizing convection combining ensemble and data assimilation techniques. Geophys. Res. Lett. 29 38-31-38-34.

Grell, G.A., Peckham, S.E., Schmitz, R., McKeen, S.A., Frost, G., Skamarock, W.C., Eder, B., 2005. Fully coupled "online" chemistry within the WRF model. Atmos. Environ. 39, 6957–6975.

Guenther, A.B., Jiang, X., Heald, C.L., Sakulyanontvittaya, T., Duhl, T., Emmons, L.K., Wang, X., 2012. The Model of Emissions of Gases and Aerosols from Nature version 2.1 (MEGAN2.1): an extended and updated framework for modeling biogenic emissions. Geosci. Model Dev. (GMD) 5, 1471–1492.

Guevara, M., Soret, A., Arévalo, G., Martínez, F., Baldasano, J.M., 2014. Implementation of plume rise and its impacts on emissions and air quality modelling. Atmos. Environ. 99, 618–629.

Hardacre, C., Wild, O., Emberson, L., 2015. An evaluation of ozone dry deposition in global scale chemistry climate models. Atmos. Chem. Phys. 15, 6419–6436.

Heald, C.L., Geddes, J.A., 2016. The impact of historical land use change from 1850 to 2000 on particulate matter and ozone. Atmos. Chem. Phys. 16, 14997–15010.

Hong, S.-Y., Noh, Y., Dudhia, J., 2006. A New Vertical Diffusion Package with an Explicit Treatment of Entrainment Processes. Mon. Weather Rev. 134, 2318–2341.

Janjic, Z., 1996. The Mellor-Yamada Level 2.5 Turbulence Closure Scheme in the NCEP Eta Model, vol. 4. World Meteorological Organization-Publications-WMO TD, pp. 14–14.15.

Janjić, Z.I., 1990. The step-mountain coordinate: physical package. Mon. Weather Rev. 118, 1429–1443.

Janjić, Z.I., 1994. The step-mountain Eta coordinate model: further developments of the convection, viscous sublayer, and turbulence closure schemes. Mon. Weather Rev. 122, 927–945.

Lai, A., Liu, Y., Chen, X., Chang, M., Fan, Q., Chan, P., Wang, X., Dai, J., 2016. Impact of land-use change on atmospheric environment using refined land surface properties in the Pearl River Delta, China. Adv. Meteorol. 2016 15.

Lelieveld, J., Dentener, F.J., 2000. What controls tropospheric ozone? J. Geophys. Res.: Atmosphere 105, 3531–3551.

Li, M., Zhang, Q., Kurokawa, J.-i., Woo, J.-H., He, K., Lu, Z., Ohara, T., Song, Y., Streets, D.G., Carmichael, G.R., Cheng, Y., Hong, C., Huo, H., Jiang, X., Kang, S., Liu, F., Su, H., Zheng, B., 2017. MIX: a mosaic Asian anthropogenic emission inventory under the international collaboration framework of the MICS-Asia and HTAP. Atmos. Chem. Phys. 17, 935–963.

Lu, X., Hong, J., Zhang, L., Cooper, O.R., Schultz, M.G., Xu, X., Wang, T., Gao, M., Zhao, Y., Zhang, Y., 2018. Severe surface ozone pollution in China: a global perspective. Environ. Sci. Technol. Lett. 5, 487–494.

Milovac, J., Warrach-Sagi, K., Behrendt, A., Späth, F., Ingwersen, J., Wulfmeyer, V., 2016. Investigation of PBL schemes combining the WRF model simulations with scanning water vapor differential absorption lidar measurements. J. Geophys. Res.: Atmosphere 121, 624–649.

Mlawer, E.J., Taubman, S.J., Brown, P.D., Iacono, M.J., Clough, S.A., 1997. Radiative transfer for inhomogeneous atmospheres: RRTM, a validated correlated-k model for the longwave. J. Geophys. Res.: Atmosphere 102, 16663–16682.

Monks, P.S., Archibald, A.T., Colette, A., Cooper, O., Coyle, M., Derwent, R., Fowler, D., Granier, C., Law, K.S., Mills, G.E., Stevenson, D.S., Tarasova, O., Thouret, V., von Schneidemesser, E., Sommariva, R., Wild, O., Williams, M.L., 2015. Tropospheric ozone and its precursors from the urban to the global scale from air quality to short-lived climate forcer. Atmos. Chem. Phys. 15, 8889–8973.

Noilhan, J., Planton, S., 1989. A simple parameterization of land surface processes for meteorological models. Mon. Weather Rev. 117, 536–549.

Pleim, J.E., Xiu, A., Finkelstein, P.L., Otte, T.L., 2001. A coupled land-surface and dry deposition model and comparison to field measurements of surface heat, moisture, and ozone fluxes. Water Air Soil Pollut. Focus 1, 243–252.

Pleim, J.E., 2006. A simple, efficient solution of flux–profile relationships in the atmospheric surface layer. J. Appl. Meteorol. Climatol. 45, 341–347.

Pleim, J.E., 2007. A combined local and nonlocal closure model for the atmospheric boundary layer. Part I: model description and testing. J. Appl. Meteorol. Climatol. 46, 1383–1395.

Park, R.J., Hong, S.K., Kwon, H.A., Kim, S., Guenther, A., Woo, J.H., Loughner, C.P., 2014. An evaluation of ozone dry deposition simulations in East Asia. Atmos. Chem. Phys. 14, 7929–7940.

Sitch, S., Cox, P.M., Collins, W.J., Huntingford, C., 2007. Indirect radiative forcing of climate change through ozone effects on the land-carbon sink. Nature 448, 791.

Song, Y., Zhang, M., Cai, X., 2006. PM10 modeling of Beijing in the winter. Atmos. Environ. 40, 4126–4136.

Stull, R.B., 1988. An Introduction to Boundary Layer Meteorology. Springer, Netherlands.

Tai, A.P., Martin, M.V., Heald, C.L., 2014. Threat to future global food security from climate change and ozone air pollution. Nat. Clim. Chang. 4, 817–821.

Tao, W., Liu, J., Ban-Weiss, G.A., Hauglustaine, D.A., Zhang, L., Zhang, Q., Cheng, Y., Yu, Y., Tao, S., 2015. Effects of urban land expansion on the regional meteorology and air quality of eastern China. Atmos. Chem. Phys. 15, 8597–8614.

Wang, L., Zhang, Y., Wang, K., Zheng, B., Zhang, Q., Wei, W., 2016. Application of weather Research and forecasting model with chemistry (WRF/chem) over northern China: sensitivity study, comparative evaluation, and policy implications. Atmos. Environ. 124, 337–350.

Wang, T., Ding, A., Gao, J., Wu, W.S., 2006. Strong ozone production in urban plumes from Beijing, China. Geophys. Res. Lett. 33, L21806.

Wesely, M.L., 1989. Parameterization of surface resistances to gaseous dry deposition in regional-scale numerical-models. Atmos. Environ. 23, 1293–1304.

Wesely, M.L., Hicks, B.B., 2000. A review of the current status of knowledge on dry deposition. Atmos. Environ. 34, 2261–2282.

Wu, Z.Y., Wang, X.M., Turnipseed, A.A., et al., 2012. Evaluation and improvements of two community models in simulating dry deposition velocities for peroxyacetyl nitrate (PAN) over a coniferous forest. J. Geophys. Res.-Atmos. 117, D04310. https://doi.org/10.1029/2011JD016751.

Xie, B., Fung, J.C.H., Chan, A., Lau, A., 2012. Evaluation of nonlocal and local planetary boundary layer schemes in the WRF model. J. Geophys. Res.: Atmosphere 117, D12103.

Yan, Y., Lin, J., He, C., 2018. Ozone trends over the United States at different times of day. Atmos. Chem. Phys. 18, 1185–1202.

Yerramilli, A., Challa, V.S., Dodla, V.B.R., Dasari, H.P., Young, J.H., Patrick, C., Baham, J.M., Hughes, R., Hardy, M.G., Swanier, S.J., 2010. Simulation of Surface Ozone Pollution in the Central Gulf Coast Region Using WRF/Chem Model: Sensitivity to PBL and Land Surface Physics. Adv. Meteorol. 24.

Young, P.J., Archibald, A.T., Bowman, K.W., Lamarque, J.F., Naik, V., Stevenson, D.S., Tilmes, S., Voulgarakis, A., Wild, O., Bergmann, D., Cameron-Smith, P., Cionni, I., Collins, W.J., Dalsøren, S.B., Doherty, R.M., Eyring, V., Faluvegi, G., Horowitz, L.W., Josse, B., Lee, Y.H., MacKenzie, I.A., Nagashima, T., Plummer, D.A., Righi, M., Rumbold, S.T., Skeie, R.B., Shindell, D.T., Strode, S.A., Sudo, K., Szopa, S., Zeng, G., 2013. Pre-industrial to end 21st century projections of tropospheric ozone from the atmospheric chemistry and climate model intercomparison project (ACCMIP). Atmos. Chem. Phys. 13, 2063–2090.

Žabkar, R., Honzak, L., Skok, G., Forkel, R., Rakovec, J., Ceglar, A., Žagar, N., 2015. Evaluation of the high resolution WRF-Chem (v3.4.1) air quality forecast and its comparison with statistical ozone predictions. Geosci. Model Dev. (GMD) 8, 2119–2137.

Zhang, D., Anthes, R.A., 1982. A high-resolution model of the planetary boundary layer—sensitivity tests and comparisons with SESAME-79 data. J. Appl. Meteorol. 21, 1594–1609.

Zhang, L.M., Brook, J.R., Vet, R., 2002. On ozone dry deposition–with emphasis on non-stomatal uptake and wet canopies. Atmos. Environ. 36, 4787–4799.

Zhang, L., Brook, J.R., Vet, R., 2003. A revised parameterization for gaseous dry deposition in air-quality models. Atmos. Chem. Phys. 3, 2067–2082.

Zhang, Q., Chang, M., Zhou, S., Chen, W., Wang, X., Liao, W., Dai, J., Wu, Z., 2017. Evaluate dry deposition velocity of the nitrogen oxides using Noah-MP physics ensemble simulations for the Dinghushan Forest, Southern China. Asia Pac. J. Atmos. Sci. 53, 519–536.

Zhao, Y., Zhang, L., Tai, A.P.K., Chen, Y., Pan, Y., 2017. Responses of surface ozone air quality to anthropogenic nitrogen deposition in the Northern Hemisphere. Atmos. Chem. Phys. 17, 9781–9796.

Zhou, M., Zhang, L., Chen, D., et al., 2019. The impact of aerosol–radiation interactions on the effectiveness of emission control measures. Environ. Res. Lett. 14, 024002.